University of Groningen

Bachelor Thesis

Astronomy

Identification of young star-forming galaxies at redshifts z=0-7

Author:
Francis H. Tang

Supervisor:
Prof. dr. Karina I. Caputi

Co-supervisor:
Laura Bisigello, PhD

July 10, 2017

Abstract

In this work we investigate the presence of young star-forming galaxies at redshifts z=0-7 using spectral energy distribution (SED) fitting. We use photometry in the CANDELS GOODS-South field, the photometric redshift code Le PHARE and galaxy SED models from the Yggdrasil package. The Yggdrasil templates have inferior performance than traditional galaxy models in estimating the redshifts of all galaxies in a flux-limited catalogue like CANDELS GOODS-S. Nevertheless, the availability of young galaxy templates with full incorporation of nebular emission in Yggdrasil is crucial to identify young galaxies with these characteristics at different redshifts. Among the galaxies in our sample with good redshift recovery, we identify 11.6% of them to be young and star-forming. Moreover, the percentage of young star-forming galaxies decreases with increasing redshift. We explore the possibility that this decrease is due to a degeneracy in the SED fitting, which may be caused by a decline in the signal-to-noise ratio of the photometry in some bands. Simulations suggests that our criterion for securely identifying young star-forming galaxies is robust.

Contents

Acknowledgements

I would like to thank my supervisor Prof. dr. Karina Caputi for her explanations, patience, helpful feedback and swift responses throughout the entire ten weeks of this research project. I would also like to thank Laura Bisigello, for immediately coming to aid whenever I got stuck, and for her understanding of the software I've been using. I wish to thank the students of the Kapteyn Institute for the good talks and lunches we had during many hours in the coffee corner, and especially Job Formsma and Sophie van Mierlo for maintaining a good working environment. Finally, I would like to thank Martijn Smeenk for his confidence in me, and my family for their continuous support and care.

1 Introduction

The goal of this work is to investigate the effect of using a family of spectral energy distribution (SED) templates with a full treatment of nebular emission lines on the identification of young star-forming galaxies at different cosmic times. To do this, we analyze photometric observations of a deep field of galaxies from ultraviolet to near-infrared wavelengths.

Galaxy formation in the early Universe
In order to understand the nature of galaxy formation in the early Universe, we need to learn about the amount and distribution of different galaxy populations. We can only obtain this kind of information from a reliable classification of various types of galaxies. The type we focus on in this work is a young galaxy in its star-forming phase. The earliest galaxies formed in the Universe are believed to contain a large number of bright, short-lived stars. These young, star-forming galaxies are characterized by a large amount of nebular emission in addition to their stellar continuum. Taking such emission lines into account when modeling galaxies at high redshift may be an essential addition to their SEDs. In this work we explore a method to identify young star-forming galaxies within a flux-limited catalogue from a blank field of the sky.

Galaxy SED fitting
Photometric observations in multiple bands can be used to determine the SED of a galaxy. A redshift determined from this SED is called a photometric redshift. Combined photometry in various bands with different wavelength ranges resemble a spectrum well enough to distinguish certain spectral features such as the Lyman (912Å) break and the 4000Å break. Naturally, these features are not seen as sharp as they would appear in a spectrum, rather they are an addition to the flux on top of the stellar continuum in certain bands.
When we want to examine these features, taking a spectrum is naturally the preferred method. However, with photometry it is possible to observe fainter objects than with spectroscopy in less time. Therefore we use photometric redshifts for treating large galaxy surveys.

In recent years the importance of the contribution of nebular emission lines to the SEDs of young galaxies gained recognition. The effects studied include physical parameters such as stellar mass, age and formation redshift (Schaerer & de Barros, 2009; Stark et al., 2014). Zackrisson et al. (2011) developed a spectral synthesis code with a full treatment of nebular emission lines, geared toward studying galaxies at high redshift.

In Section 2 I describe the datasets used and summarize my work methodology. In Section 3 I present my results: photometric redshifts obtained by SED fitting, their dependence on the signal-to-noise ratio of the photometry, and the identification of a robust set of young star-forming galaxies. My conclusions are discussed in Section 4.
Throughout this work, we use AB magnitudes (Oke & Gunn, 1983), and assume a cosmology with $H_0 = 70$ km s^{-1} Mpc^{-1} and a flat Universe with $\Omega_m = 0.3$ and $\Omega_\Lambda = 0.7$.

2 Data and Methodology

2.1 Photometric catalogue

All results in this work are based on the publicly available Cosmic Assembly Near-infrared Deep Extragalactic Legacy (*CANDELS*) survey (Grogin et al., 2011; Koekemoer et al., 2011), in particular the South ('S') field of the Great Observatories Origins Deep Survey (*GOODS*) (Guo et al., 2013). Among these Great Observatories are the *Hubble Space Telescope* (*HST*), *Spitzer* and *Chandra*, some of the world's most high-end telescopes.
The observations in the CANDELS GOODS-S field are among the deepest and richest to date, which makes it an excellent field to study cosmic star formation history, galaxy formation and galaxy evolution.
In this study we use CANDELS photometry from 15 filters, ranging from ultraviolet (UV) to near-infrared (NIR) wavelengths, which are listed in Table 1. In total, 17 filters were used for the observations, including *HST*'s infrared Wide Field Camera 3 (*HST/WFC3*) and optical Advanced Camera for Surveys (*HST/ACS*). Data from two *IRAC* filters (5.8 and 8.0 μm) is left out of our analysis, because their photometry is less sensitive than the other bands. Additionally, *Le PHARE* could confuse radiation of such wavelengths with infrared dust emission at low redshift.
The CANDELS catalogue covers 173 arcmin^2 centered at RA $03^h32^m30^s$, dec -27°48^m20^s (Equatorial J2000), and contains 34930 objects.

Instrument	Band	Effective wavelength
CTIO	U	3715 Å
VIMOS	U	3766 Å
HST/ACS	F435W	4316 Å
	F606W	5733 Å
	F775W	7634 Å
	F814W	7864 Å
	F850LP	8974 Å
HST/WFC3	F098M	9802 Å
	F105W	1.04 μm
	F125W	1.23 μm
	F160W	1.58 μm
ISAAC	Ks	2.15 μm
HAWKI	Ks	2.13 μm
Spitzer/IRAC	CH1	3.51 μm
	CH2	4.44 μm

Table 1: Filters from the CANDELS survey of which the photometry is used in this research. The bands cover UV (*CTIO, VIMOS*), optical (*HST/ACS*) and NIR (*HST/WFC3* up to *IRAC*) wavelengths.

2.2 Software: photometric redshift computation

In order to obtain photometric redshifts for our sources, we use a public set of Fortran programs called *Le PHARE* (PHotometric Analysis for Redshift Estimations) (Arnouts et al., 1999; Ilbert et al., 2006). This software package calculates redshifts by combining photometric data and models of spectral energy distributions.

Le PHARE is composed of three parts or phases, of which only the first two are relevant for this research:

- A phase for the set-up, which includes selection of SED models, a set of filters and computation of theoretical magnitudes using these settings;
- A program that computes the photometric redshifts of an input dataset;
- A simulation program for generating catalogues (not of interest here).

In the first phase, libraries containing the theoretical magnitudes are constructed using galaxy SED templates and filter transmission curves. A transmission curve describes the fraction of light received as a function of wavelength, and is instrument- and temperature-dependent. *Le PHARE* comes with a standard package of transmission curves for various filters. The remaining ones were found in the SVO filter profile service (Rodrigo et al., 2012).

Emission lines

A key point in this research is to investigate how the contribution of nebular emission lines affects photometric redshift determination. *Le PHARE* comes with the option to add the most prominent emission lines[1] to the provided templates. Because we want full control about which lines are used, we choose to have *Le PHARE not* put emission lines into our templates. In the next section we elaborate on which templates are used in this research.

Configuration

Before running *Le PHARE*, the input catalogue is formatted to fit how *Le PHARE* expects it to be. Objects that are not observed in a band[2] have their flux and error set to (-99.9, -99.9) in that band, instead of the CANDELS standard of (-99.0, -99.0). Limiting magnitudes are applied on non-detections and the catalogue is corrected for galactic extinction. We convert fluxes to magnitudes throughout the catalogue. In addition, we set a lower limit on the error to avoid an overestimated accuracy. The minimum error is set to be 0.05 mag in the first 13 bands, and to 0.1 mag in the two *IRAC* bands. In Table 2 we list a number of parameters that are used to configure *Le PHARE*.

[1] Hα, Hβ, [OIII] and [OII]

[2] i.e. there is a lack of coverage: not the entire area of the GOODS-S field was observed in all filters, so there is an incomplete overlap.

Parameter	Values
Redshift [z_{min}, z_{max}, dz]	[0, 7, 0.01]
Extinction law	Calzetti[a]
E(B-V)	0.0, 0.05, 0.1, 0.2, 0.3, 0.5, 0.8, 1.0
Metallicity	$Z_{\odot}$

Table 2: Parameters specified in *Le PHARE* for the calculation of photometric redshifts. [a]Calzetti et al. (2000)

2.3 SED fitting

In this work we use a set of SED models from the Yggdrasil package (Zackrisson et al., 2011), a spectral synthesis code aimed at modeling high-redshift galaxies which include a more complex set of nebular emission lines than *Le PHARE*. The templates correspond to galaxies with a constant star formation rate (SFR) up until a certain age, after which the SFR drops to zero.
Despite their somewhat simplistic step-function star formation history (SFH), these SED models carry an important advantage: unlike traditional templates such as those presented by Bruzual and Charlot (2003), the Yggdrasil templates include an extensive set of emission lines (see Figure 1). The emission lines are a significant addition to the continuum radiation, especially for young star-forming galaxies at high redshift. That is why the Yggdrasil templates are well-suited for use on high redshift samples of galaxies which are expected to be young, such as done by Ström (2012), Rydberg et al. (2015) and Bisigello et al. (2017). Here, we extend the use of the templates to a wider range of redshifts, z=0-7, to find out whether they produce sensible results with a more general sample, too.

Although we use the Yggdrasil templates throughout this work, we obtain photometric redshifts both with Yggdrasil and Bruzual&Charlot templates to investigate the overall performance of these template families in the determination of photometric redshifts.
The relevant properties of the Yggdrasil and Bruzual&Charlot templates we use are listed in Table 4, and the templates' ages ranging from 50 Myr to 12 Gyr can be found in Table 3. In order to be consistent in controlling the effect of emission lines, none were added to the Bruzual&Charlot templates while running *Le PHARE* with them.

Model number	1	2	3	4	5	6	7	8	9	10	11	12
Age (Gyr)	0.05	0.2	0.4	0.6	0.8	1.0	1.2	1.5	2.0	4.0	8.0	12.0

Table 3: The age in units of 10^9 years of the SED templates used in this work.

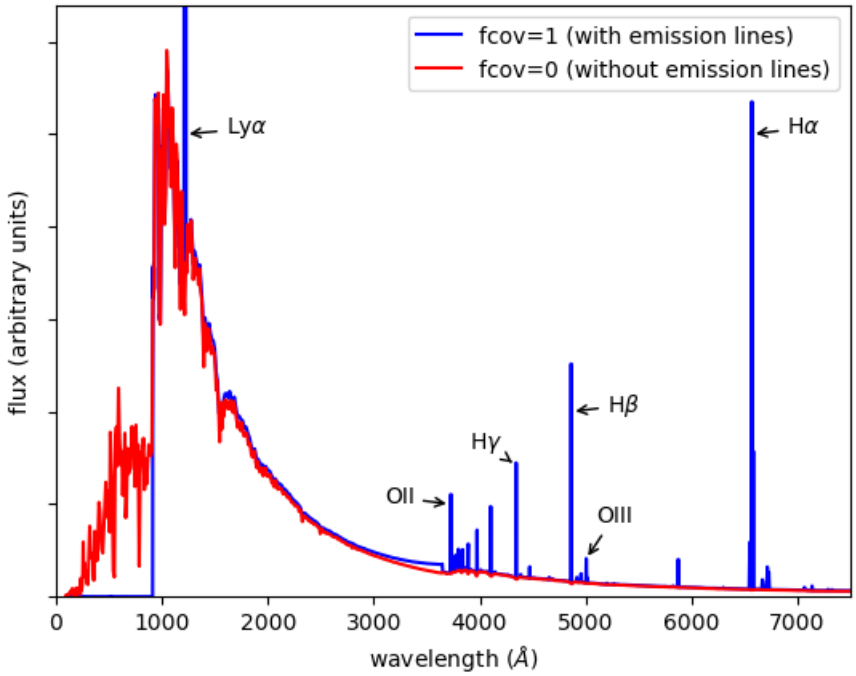

Figure 1: The SED of two Yggdrasil templates of age 50 Myr. The blue line is a template with emission lines (f_{cov}=1), the red line is one without emission lines (f_{cov}=0). The most prominent lines are indicated. Note that the Lyman α (Lyα) line extends above the figure boundaries.

Parameter	Values (Ygg a)	Values (Ygg b)	Values (BC03)
SFH type	step-function	step-function	declining[a]
$\tau_{\rm SFH}$ (Gyr)	0.1	0.1	0.1, 1, 10
f_{cov}	1	0[b]	-

Table 4: Properties of the SED templates. Ygg a denotes the run with the Yggdrasil templates including emission lines, Ygg b the run without emission lines in the youngest template, and BC03 are the Bruzual and Charlot (2003) templates.
[a]SFH $\propto \exp^{-t/\tau}$
[b]$f_{cov} = 0$ only for the youngest template (model number 1, age 50 Myr)

3 Results

In the following sections the results from *Le PHARE*'s photometric redshift computation are discussed, along with a number of criteria for the identification of a robust set of young, star-forming galaxies.
The parameters of the output from *Le PHARE* that we use in this section, are:

1. ID: the identification number of the object, same as in the input catalogue.
2. z_{phot}: the best estimate (best solution) for the photometric redshift.
3. $\chi^2_{\rm red}$: the reduced value of χ^2 corresponding to the best solution.
4. Model number: the SED template used to find the best solution.
5. N_{bands}: The number of photometric bands that were used to determine the best solution.

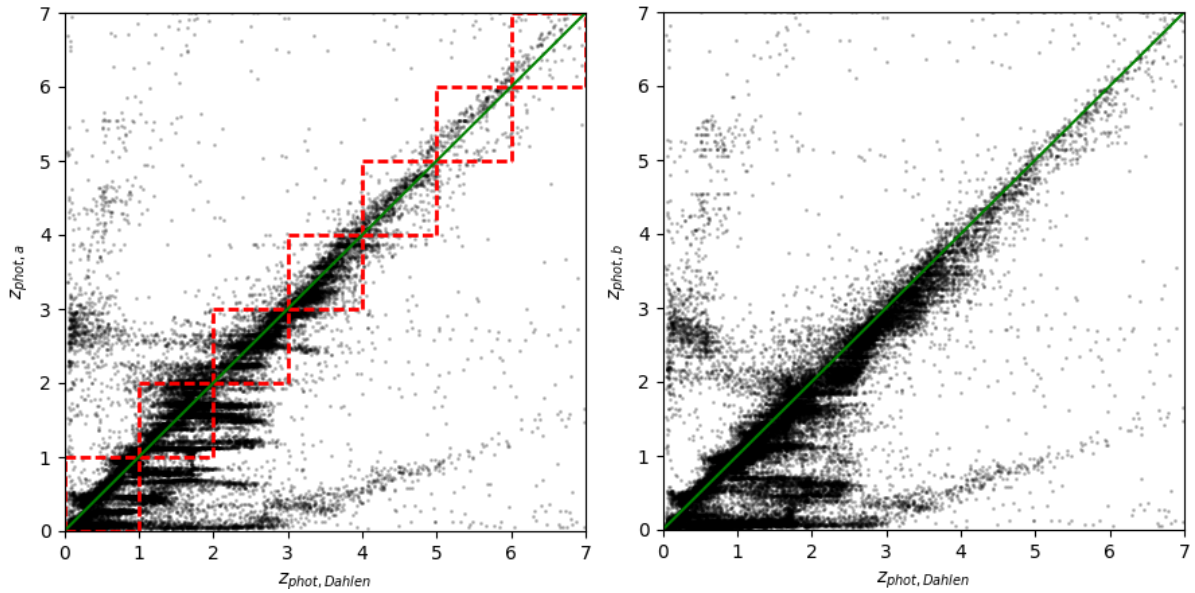

Figure 2: Left: The photometric redshifts as computed by *Le PHARE* in *run a*, compared to those computed by Dahlen et al. (2013). In green the identity line is shown. In red, redshift bins of size 1 are indicated. The objects within those bins are selected for further analysis.
Right: The same plot, but with the results of *run b* on the vertical axis.

3.1 *Le PHARE* photometric redshifts

In this section we compare photometric redshifts obtained with three different sets of templates: Yggdrasil templates with emission lines, which we call "*run a*", Yggdrasil templates without emission lines ("*run b*") and Bruzual&Charlot templates (see Table 4). Our photometric redshifts are plotted against a set of photometric redshifts by Dahlen

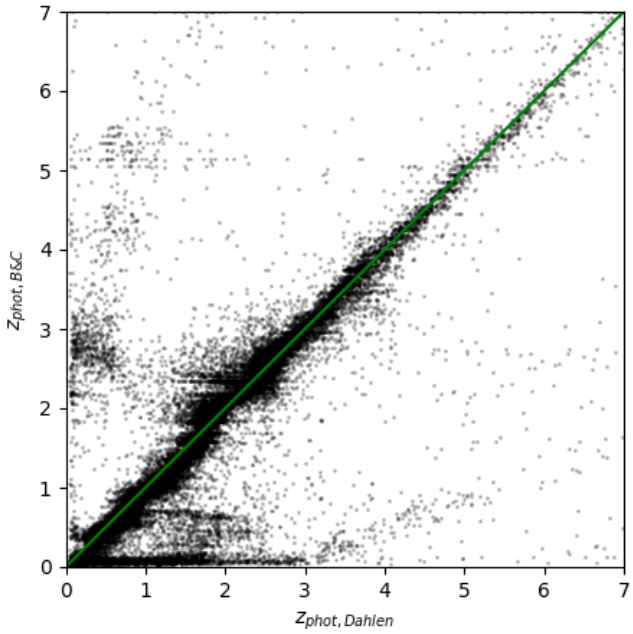

Figure 3: Photometric redshifts as computed by *Le PHARE* in a reference run with templates from Bruzual and Charlot (2003) (see Table 4).

et al. (2013). They combine photometric redshifts found by 11 different studies in the CANDELS GOODS-S field into a mean photometric redshift, creating a robust dataset that we utilize here to compare our own results with.
The Dahlen et al. (2013) redshifts cover a range of z_{Dahlen}=0-10, while our research focuses on the range z=0-7. Selecting the Dahlen reference redshifts in the range z_{Dahlen}=0-7, we continue our analysis on 34587 out of the 34930 CANDELS objects.

Redshifts from "*run a*"
Figure 2 (left) shows the photometric redshift as determined by *Le PHARE* in *run a* against the Dahlen set of photometric redshifts. The purpose of the red dashed lines plotted around the identity line will be discussed in the next section.
A feature that stands out immediately in this plot is the collection of horizontal stripes at redshifts $z_{phot,a} < 2$.
Additionally, two 'arms' are extending above and below the main collection of redshifts along the identity line. These features are probably originating from a degeneracy in the identification of the Lyman and 4000Å break, two well-known spectral breaks in galaxy SEDs. This degeneracy means that in the redshift fitting, either the Lyman break (at 912Å) is treated as being the 4000Å break, resulting in a slight systematic overestimation of the redshift associated with that object, or the other way around, resulting in a systematic underestimation of the redshift. The lower arm shows most clearly, while the upper arm has a more cloud-like appearance.
Moreover, our redshifts above z=5 are slightly overestimated, as they can be seen to lie

just next to the identity line. This deviation may be explained by the fact that most of the photometric redshifts in Dahlen et al. (2013) have been obtained without including emission lines, while ours do include them.

The level of agreement between two samples of redshifts can be measured using the fraction of outliers and the root mean square (rms) deviation $(\delta z)_{rms}$, determined from the scatter in redshift δz:

$$\delta z = \frac{|z_{phot} - z_{ref}|}{1 + z_{ref}}, \tag{1}$$

where z_{phot} is the photometric redshift as calculated by *Le PHARE*, and z_{ref} is the reference redshift, in this case $z_{phot,Dahlen}$. The fraction of 'outliers' is taken to be the fraction of objects that satisfy $\delta z \geq 0.15$. We determine an rms deviation of $(\delta z)_{rms} = 0.039$ for *run a*, calculated after excluding the 35.5% of objects that are outliers. We recognize that this is a relatively large fraction of outliers, but want to remind the reader that this is an exploratory study to investigate the overall performance of the Yggdrasil templates on a blank catalogue.

Redshifts from "*run b*"

Figure 2 (right) shows the photometric redshifts as determined by *Le PHARE* in *run b* against the Dahlen set of photometric redshifts. This run is performed to find out whether the youngest template in *run a* with nebular emission lines is significantly better than a young template without them. *Run b* has the same *Le PHARE* settings as *run a* (see Table 4), except for a covering factor $f_{cov} = 0$ in the template of age 50 Myr, effectively letting interstellar gas absorb all line emission.

In the *run b* plot, we recognize the same systematic under- and overestimations where the Lyα and 4000Å break are interchanged in the SED fitting. The horizontal features at lower redshifts are less clear, while the cloud-like structure around $2 \leq z_{phot,a} \leq 3$ and $0 \leq z_{phot,Dahlen} \leq 1$ is more pronounced. The slight overestimation of most redshifts at $z_{phot,a} \geq 5$ has disappeared. This strengthens our belief that the incorporation of emission lines has an effect on the photometric redshift determination of at high redshifts. The *run b* plot has a fraction of outliers equal to 32.4%. After excluding these objects, we find that $(\delta z)_{rms} = 0.039$ for the 'good' objects in this run as well.

Redshifts from Bruzual&Charlot

In Figure 3 we plot the photometric redshifts as determined by *Le PHARE* with the Bruzual&Charlot templates (see Table 4) against the Dahlen redshifts. We recognize the same supposed degeneracy between the identification of the Lyman break and the 4000Å break, manifested as two arms extending above and below the identity line. Additionally, we see some horizontal structure at low $z_{phot,B\&C}$, similar to the two Yggdrasil results.

The main difference between the results using the Yggdrasil templates and the Bruzual&Charlot templates is the smaller amount of scatter at low redshifts. Indeed, we find a slightly lower rms error of $(\delta z)_{rms} = 0.035$, after excluding 17.8% of outliers, for the photometric redshifts

determined using the Bruzual&Charlot templates. This indicates a better agreement of the Bruzual&Charlot photometric redshifts with those from Dahlen et al. (2013).

Despite their higher fraction of outliers, we continue our analysis with the results from the Yggdrasil templates. Although the traditional Bruzual&Charlot templates appear to be the logical choice, we remind the reader that this work is a pilot study on how well we can identify young star-forming galaxies in a general sample by SED fitting, using a family of SEDs that include a full treatment of nebular emission lines.

3.2 Selection of young star-forming galaxies

We apply a number of selection criteria in order to identify young, star-forming galaxies within our sample. After each step, the number of galaxies within our selection decreases, until we get a reliably classified of 'securely' young, star-forming galaxies. The results of this Section and Section 3.4 are summarized in Table 5.

First of all, we divide the results into seven redshift bins. An indication of the distribution of photometric redshifts can be seen in Figure 2 for two runs with the Yggdrasil templates, and in Figure 3 for a run with the more traditional Bruzual and Charlot (2003) templates. Within the seven redshift squares indicated in Figure 2, 24547 objects are contained, i.e. 71% of the original sample. Hereafter, this set of 24547 sources will be referred to as our analysis sample.

Secondly, we consider 'young' galaxy candidates to be those that choose the youngest Yggdrasil SED template with emission lines (*run a*) as best solution. This template is the only one corresponding to a galaxy that is still in its star-forming phase. These sources are the ones that we isolate for further analysis. 15503 out of 24547 galaxies in our sample choose this template, i.e. 63% of the analysis sample. For the redshift distribution of these young star-forming galaxies, see the fourth column of Table 5.

Moreover, we apply a third criterion to isolate a secure subsample of the young star-forming galaxies described in the previous paragraph. We consider the set of securely young star-forming galaxies to be those that prefer the youngest template with emission lines significantly to all other templates. We quantify this criterion as follows. If the reduced value of χ^2 of the young solution (from *run a*) of a source is 1σ higher than $\chi^2_{\rm red}$ of the second best solution (*run b*), then the source is a candidate for being a securely young star-forming galaxy.

$$\Delta\chi^2_{\rm red} \equiv \frac{\chi^2_b - \chi^2_a}{\mathrm{N}_{bands} - 1} \geq 1, \tag{2}$$

where N_{bands} is the number of filters used to determine the best solution, here used to normalize $\Delta\chi^2_{\rm red}$. The value of $\Delta\chi^2_{\rm red} \geq 1$ then corresponds to a 1σ significance of the result. We find that 3254 sources satisfy this condition, and therefore 13.3% of all galaxies in our

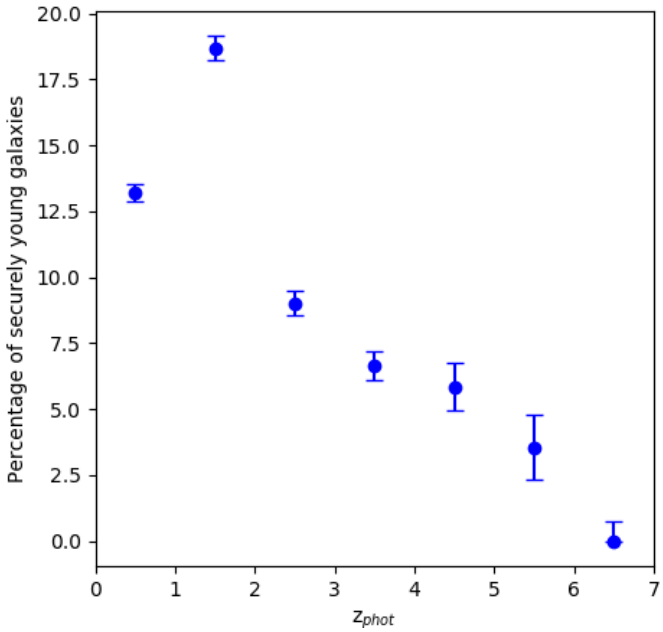

Figure 4: The secure fraction (in %) of young star-forming galaxy candidates within our sample, as a function of redshift. The error bars are derived from a binomial distribution, treating the galaxies classified as securely young star-forming as 'successes', and the not-securely young star-forming ones as 'failures'.

sample are considered to be securely young star-forming galaxy candidates (see Table 5). In the next paragraphs, we discuss the sample obtained from the aforementioned selection criteria. Thereafter, in Section 3.4, we describe a final selection criterion that improves the reliability of our classification even more.

In Figure 4 we plot the percentage of securely young star-forming galaxies in each redshift bin. From redshift 0 to 2, this percentage increases. At $z > 2$ the fraction starts to decrease steadily until it reaches 0 in the highest redshift bin.
On the basis of galaxy evolution models we would expect the fraction of young, star-forming galaxies to be highest at early cosmic times, or high redshift, and to decrease gradually as the Universe grows older. Therefore we believe that the two points at lowest redshift display the expected behaviour, especially considering the fact that those two bins encompass 75% of the lifetime of the Universe (see the last column of Table 5).

The fractional decrease in star-forming galaxies with redshift instead is a somewhat counterintuitive result, which we believe to originate from a degeneracy in the SED fitting. At higher redshift, we suspect the signal-to-noise ratio (S/N) to be lower on average. For a lower S/N, the photometric error bars are larger, the SED fitting becomes more degenerate, or in other words, the classification of galaxies having a certain age becomes less effective. This makes the identification of young star-forming galaxies more difficult, in the sense

that it is harder to obtain a robust classification. This could explain the sudden drop in the number of galaxies after the selection criterion with $\Delta\chi^2_{\mathrm{red}}$. In order to test this hypothesis, we investigate the S/N of our securely young star-forming galaxy candidates in the next section.

3.3 Dependence on the signal-to-noise ratio

In this section, we investigate the S/N of the securely young star-forming sample of galaxies compared to the S/N of the full set. We aim to find an explanation for the decrease in the fraction of young star-forming galaxies, as is shown in Figure 4. We use the photometric data of the *HST* F160W and F435W bands in this comparison. The F160W filter (IR wavelengths) is most representative of the photometry because the CANDELS catalogue is based on observations in it. The F435W band (optical, mainly blue wavelengths) is chosen because it reflects the behaviour of the photometry at shorter wavelengths.

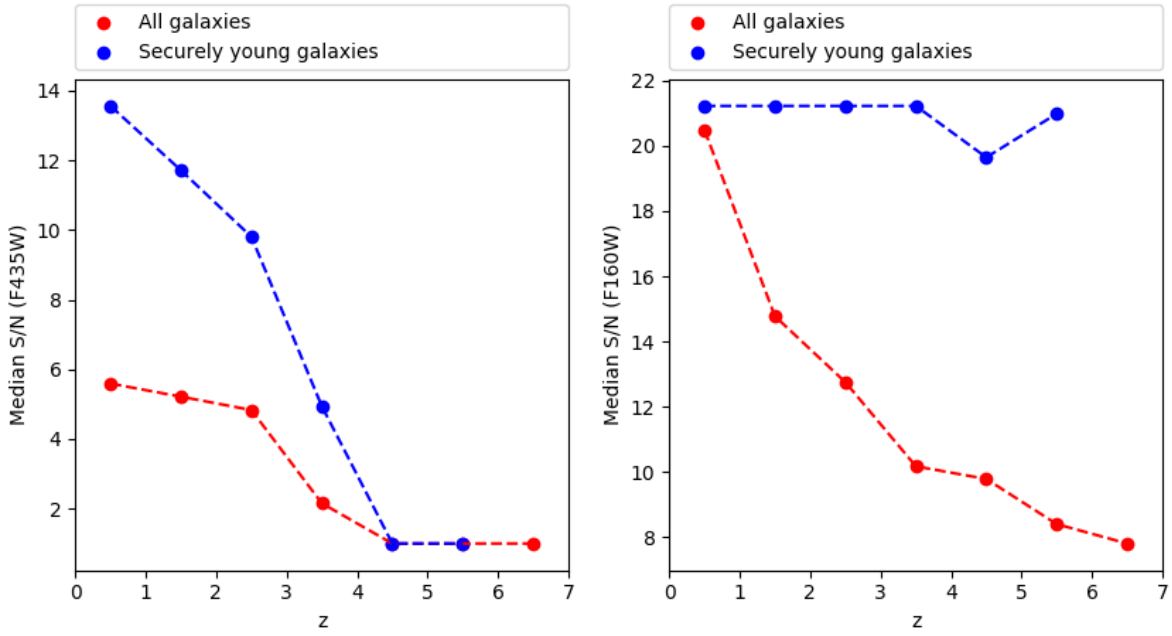

Figure 5: The median S/N of each redshift bin in the F435W filter (left) and in the F160W filter (right). Note that no value is plotted for the last redshift bin of the subsample, since it does not contain any objects.

We find the mean S/N of the securely young star-forming set to be higher than the mean S/N of the full sample (see Figure 5). This indicates that our securely young star-forming sample has a higher overall quality of its photometry. The maximum S/N at which the mean S/N of almost all securely young star-forming galaxies lie is explained as follows. The minimum error in magnitudes applied to our photometric catalogue (see section 2.2)

implies a maximum S/N for each object of

$$\left(\frac{S}{N}\right)_{max} = \frac{1}{10^{\delta \mathrm{m}/2.5} - 1} \approx 21.2 \text{ for } \delta \mathrm{m} = 0.05. \tag{3}$$

As a result, all sources with a S/N originally higher than 21.2 will be set to S/N = 21.2.

Comparing the two plots of Figure 5 we see that the S/N on average is much higher in the F160W band than in the F435W band. In both filters, our sample of securely young star-forming galaxies has a higher S/N on average. Objects beyond z=4 have a median S/N of 1 in the F435W band, which suggests that the majority of objects in this band are non-detections (we set the S/N of the non-detections to 1). This is a plausible result, because at such redshifts the F435W band detects radiation with a rest-frame wavelength below the Lyman break, where most of it is absorbed by neutral hydrogen gas. The fact that a number of the bluer bands have such low S/N indicates that the SED fitting may be more difficult at high redshifts, because there *Le PHARE* only uses a smaller number of bands. This could in part explain the decreasing fraction of securely young star-forming galaxies at high redshift.

Redshift	N_{Dahlen}	$N_{in\ bins}$	N_{young}	$N_{sec.\ young}$	$N_{rob.\ young}$	Age[a] (Gyr)
$0 \leq z < 1$	11377	9945	3259	1313	1177	5.75
$1 \leq z < 2$	11546	7466	5694	1395	1225	3.22
$2 \leq z < 3$	6780	3915	3554	353	295	2.11
$3 \leq z < 4$	3238	2212	2080	147	118	1.51
$4 \leq z < 5$	1031	650	611	38	34	1.15
$5 \leq z < 6$	401	226	194	8	5	0.92
$6 \leq z \leq 7$	214	133	111	0	0	0.75
Total	**34587**	**24547**	**15503**	**3254**	**2854**	**13.46**[b]
Percentage		100%	63.2%	13.3%	11.6%	

Table 5: The amount of CANDELS sources in seven equally sized redshift bins. The N_{Dahlen} column contains the redshift distribution of objects according to Dahlen et al. (2013). $N_{in\ bins}$ is the column with objects contained in the red squares of Figure 2. N_{young} are the objects with the youngest template with emission lines as best solution in *run a*. $N_{sec.\ young}$ are the objects classified as securely young star-forming (see Section 3.2). $N_{rob.\ young}$ are the objects classified as securely young star-forming in more than 50% of the simulations, i.e. the 'robust' young star-forming objects (see Section 3.4).
[a]Age of the Universe at the redshift of the upper limit of the bin.
[b]Current age of the Universe, so at z=0.

3.4 Simulations

As a final method to improve the robustness of our results, we run a simulation of similar photometry through *Le PHARE*, using the same configuration as described in Section 2.2. We randomize the photometry by replacing the flux of the original CANDELS catalogue with a random value inside its error bar, drawn from a uniform distribution. Because objects with a low S/N have a higher chance of their flux changing by a significant amount, those objects are expected to be classified differently than in the original results.

A total of ten simulations are performed. The securely young star-forming objects are isolated in the same way as before. After this, the IDs of these securely young galaxies in the simulations are matched to the IDs of the original (real) securely young star-forming candidates. We then count in how many of the ten simulations the original securely young star-forming objects are classified as securely young and star-forming, again. a result of 1/10 means we don't trust this classification at all, 10/10 means the classification is nice and robust.

The results are plotted as histograms for the first six redshift bins in Figure 7. As can be seen in Table 5, the seventh redshift bin does not contain any securely young objects.

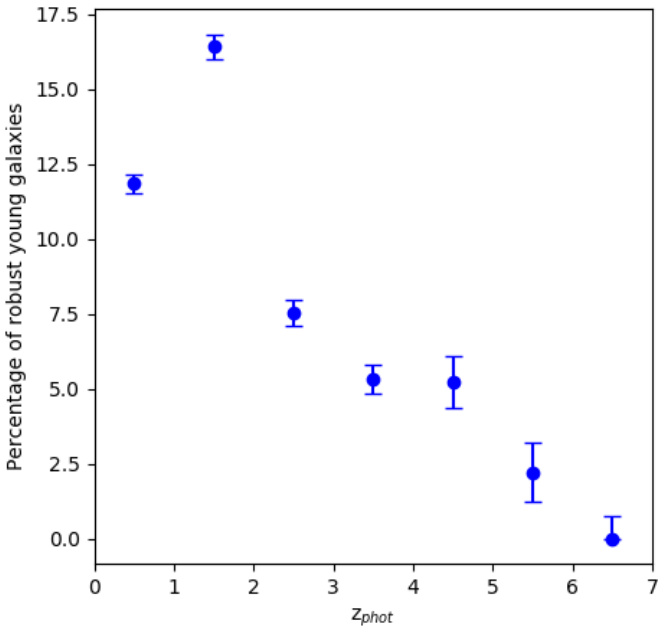

Figure 6: The robust fraction (in %) of young star-forming galaxy candidates within our analysis sample, as a function of redshift.

Therefore this last bin is left out of Figure 7. The distribution of the amount of young, star-forming galaxies does not change significantly in the lower three bins. However, at higher redshift the amount of objects in the bins becomes small enough for the relation to break down.
The majority of securely young star-forming galaxies are classified as such in each one of the ten simulations, which leads us to believe that the selection made of the securely young star-forming sources was a relatively robust one already.

Our last selection criterion will be to select all galaxies that (1) are securely young star-forming in the original run, and (2) are classified as securely young star-forming in more than half of the simulations. We consider the set of galaxies that satisfy these conditions to be robust young star-forming galaxies. The resulting amount of robust young, star-forming galaxies is 2854 out of our original set of 24547 objects, or 11.6%. The number of sources per redshift bin can be found in Table 5, and the percentage per redshift bin is shown in Figure 6.
Investigating this Figure and comparing its shape to that of Figure 4, we find that our last selection criterion did not significantly change the distribution in redshift of our candidates for young star-forming galaxies. This result indicates that our initial criterion based on $\Delta\chi^2_{\rm red}$ is a robust method for selecting young star-forming galaxies from a blind sample.

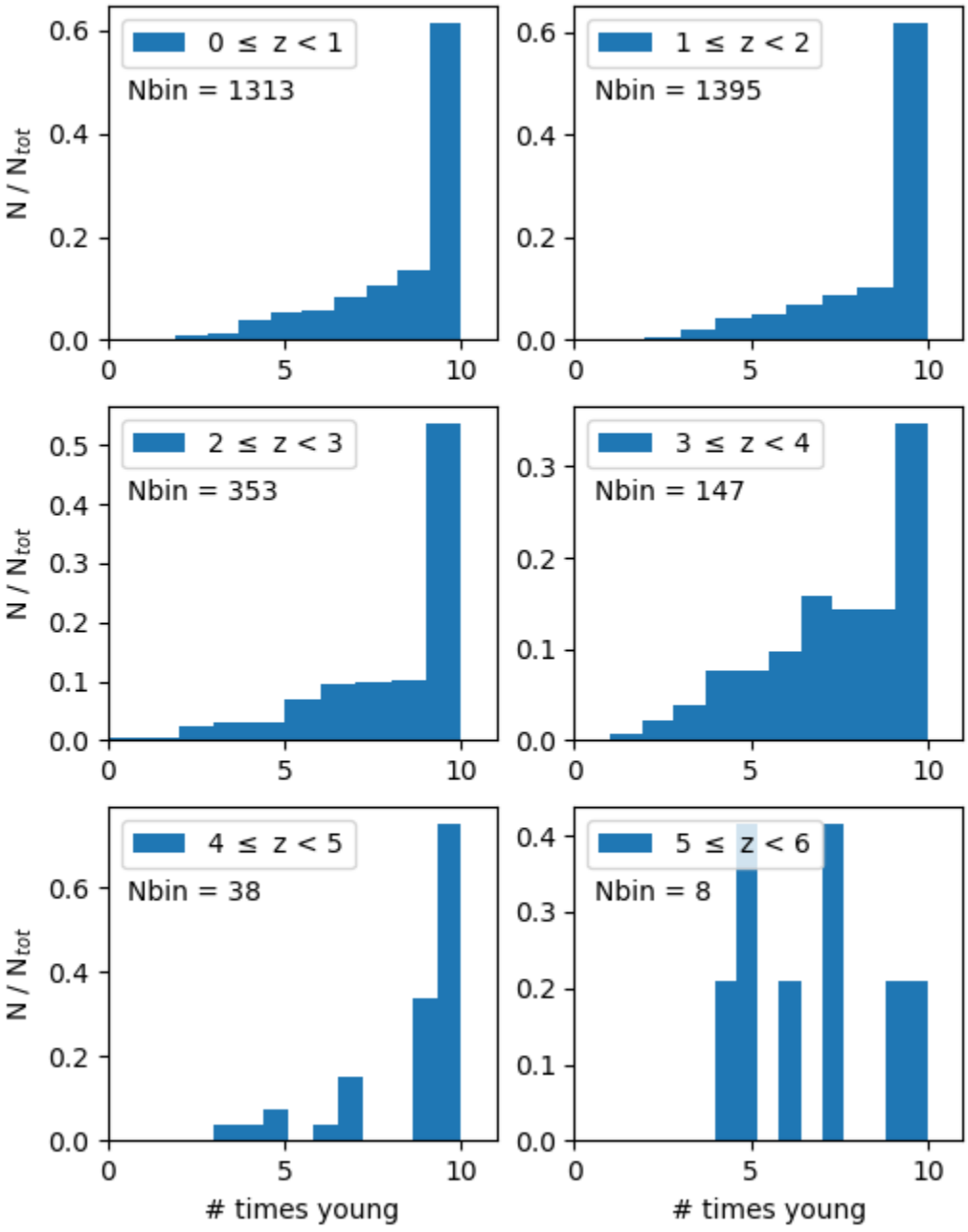

Figure 7: Histograms of the amount of times galaxies are found to be securely young and star-forming out of the ten simulations. Only the first six redshift bins are shown. The histograms are normalized to the total number of objects in each bin. Nbin denotes the total number of objects in the corresponding redshift bin.

4 Conclusions

In this study, we use the photometric redshift code *Le PHARE* (Arnouts et al., 1999; Ilbert et al., 2006) and galaxy SED models from the Yggdrasil package (Zackrisson et al., 2011) to determine photometric redshifts for 34587 sources in the CANDELS GOODS-S field (Guo et al., 2013). We apply a number of selection criteria to identify a robust subsample of young, star-forming galaxies.

A comparison of photometric redshifts obtained with Yggdrasil templates, both with (*run a*) and without (*run b*) emission lines, to photometric redshifts obtained by Dahlen et al. (2013) shows that the Yggdrasil templates perform well at redshifts z > 4 (see Figure 2). In the range z=0-7 we found rms deviations (see Section 3.1) of $(\delta z)_{rms} = 0.039$ for both Yggdrasil results (determined while excluding a fraction of outliers of 35.5% and 32.4% for *run a* and *run b*, respectively). With a smaller outlier fraction of OLF = 17.8% and $(\delta z)_{rms} = 0.035$, our reference templates from Bruzual and Charlot (2003) show a better overall performance. We conclude that the Bruzual&Charlot templates are better suited for computing redshifts for general blank field catalogues than the Yggdrasil templates.

We select galaxies within seven redshift bins (see Figure 2) and isolate those satisfying $\Delta\chi^2_{\rm red} \geq 1$ (see Section 3.2) in more than 50% of our simulations. We find that 11.6% of the sources in our sample can be reliably classified as young star-forming galaxies. Our results indicate that the fraction of supposed young star-forming galaxies decreases with increasing redshift (see Figures 4 and 6). The different behaviors in S/N as a function of redshift of the subsample of young star-forming galaxies and the analysis sample (see Figure 5) suggest that this effect may in part be caused by degenerate SED fitting, rather than a low S/N within the subset. Nevertheless, a more complete analysis of the photometry and $\chi^2_{\rm red}$ of the different samples of galaxies needs to be done in order to confirm this.

Another possible effect that could cause the fractional decrease in young star-forming galaxies as a function of redshift may be an incomplete representation of stellar mass and galaxy luminosities at high redshift. Sources at high redshift have a fainter apparent magnitude, which may cause us to only observe the brightest, most massive galaxies of a population at high z, while we observe the full population at low z. In this work we did not apply stellar mass or luminosity cuts, therefore this effect is not accounted for.

The relatively small difference in the fractions of young star-forming galaxy candidates before and after the simulations criterion is applied (from 13.3% to 11.6%), indicates that our initial selection criterion for the 'securely' young, star-forming galaxies is robust in itself. We do not expect the fraction of securely young star-forming galaxy candidates to change significantly if a larger number of simulations were done.

References

Arnouts, S., Moscardini, L., Matarrese, S., Lucchin, F., Fontana, A., & Giallongo, E. (1999). Measuring and modelling the redshift evolution of clustering: the Hubble Deep Field North. *MNRAS*, *310*, 540–556.

Bisigello, L., Caputi, K. I., Colina, L., Le Fèvre, O., Nørgaard-Nielsen, H. U., Pérez-González, P. G., ... Koekemoer, A. (2017). Recovering the properties of high redshift galaxies with different JWST broad-band filters. *ArXiv e-prints*.

Bruzual, G. & Charlot, S. (2003). Stellar population synthesis at the resolution of 2003. *MNRAS*, *344*, 1000–1028.

Calzetti, D., Armus, L., Bohlin, R. C., Kinney, A. L., Koornneef, J., & Storchi-Bergmann, T. (2000). The Dust Content and Opacity of Actively Star-forming Galaxies. *ApJ*, *533*, 682–695.

Dahlen, T., Mobasher, B., Faber, S. M., Ferguson, H. C., Barro, G., Finkelstein, S. L., ... Wilson, G. (2013). A Critical Assessment of Photometric Redshift Methods: A CANDELS Investigation. *ApJ*, *775*, 93.

Grogin, N. A., Kocevski, D. D., Faber, S. M., Ferguson, H. C., Koekemoer, A. M., Riess, A. G., ... Yun, M. S. (2011). CANDELS: The Cosmic Assembly Near-infrared Deep Extragalactic Legacy Survey. *ApJ*, *197*, 35.

Guo, Y., Ferguson, H. C., Giavalisco, M., Barro, G., Willner, S. P., Ashby, M. L. N., ... van der Wel, A. (2013). CANDELS Multi-wavelength Catalogs: Source Detection and Photometry in the GOODS-South Field. *ApJ*, *207*, 24.

Ilbert, O., Arnouts, S., McCracken, H. J., Bolzonella, M., Bertin, E., Le Fèvre, O., ... Vergani, D. (2006). Accurate photometric redshifts for the CFHT legacy survey calibrated using the VIMOS VLT deep survey. *A&A*, *457*, 841–856.

Koekemoer, A. M., Faber, S. M., Ferguson, H. C., Grogin, N. A., Kocevski, D. D., Koo, D. C., ... Yun, M. S. (2011). CANDELS: The Cosmic Assembly Near-infrared Deep Extragalactic Legacy Survey - The Hubble Space Telescope Observations, Imaging Data Products, and Mosaics. *ApJ*, *197*, 36.

Oke, J. B. & Gunn, J. E. (1983). Secondary standard stars for absolute spectrophotometry. *ApJ*, *266*.

Rodrigo, C. et al. (2012). SVO Filter Profile Service. Retrieved from http://svo2.cab.inta-csic.es/theory/fps/

Rydberg, C.-E., Zackrisson, E., Zitrin, A., Guaita, L., Melinder, J., Asadi, S., ... Ström, T. (2015). A Search for Population III Galaxies in CLASH. I. Singly-imaged Candidates at High Redshift. *ApJ*, *804*, 13.

Schaerer, D. & de Barros, S. (2009). The impact of nebular emission on the ages of $z \approx 6$ galaxies. *A&A*, *502*, 423–426.

Stark, D. P., Richard, J., Siana, B., Charlot, S., Freeman, W. R., Gutkin, J., ... Milvang-Jensen, B. (2014). Ultraviolet emission lines in young low-mass galaxies at $z \simeq 2$: physical properties and implications for studies at $z > 7$. *MNRAS*, *445*, 3200–3220.

Ström, T. (2012). Hunting for Primordial Galaxies. *Master Thesis, University of Stockholm*.

Zackrisson, E. et al. (2011). The Spectral Evolution of the First Galaxies. I. James Webb Space Telescope Detection Limits and Color Criteria for Population III Galaxies. *ApJ*, *740*, 13.